Published in final edited form as:
Neuroimage. 2010 October 1; 52(4): 1224–1229. doi:10.1016/j.neuroimage.2010.05.060.

Topographic Organization of V1 Projections through the Corpus Callosum in Humans

M Saenz[1,2] and **I Fine**[3]

[1]Department of Clinical Neuroscience, CHUV Hospital, University of Lausanne, Switzerland [2]Division of Biology, California Institute of Technology, Pasadena, California 91125 [3]Department of Psychology, University of Washington, Seattle, Washington 98195

Abstract

The visual cortex in each hemisphere is linked to the opposite hemisphere by axonal projections that pass through the splenium of the corpus callosum. Visual callosal connections in humans and macaques are found along the V1/V2 border where the vertical meridian is represented. Here we identify the topography of V1 vertical midline projections through the splenium within six human subjects with normal vision using diffusion-weighted MR imaging and probabilistic diffusion tractography. Tractography seed points within the splenium were classified according to their estimated connectivity profiles to topographic subregions of V1, as defined by functional retinotopic mapping. First, we report a ventral-dorsal mapping within the splenium with fibers from ventral V1 (representing the upper visual field) projecting to the inferior-anterior corner of the splenium and fibers from dorsal V1 (representing the lower visual field) projecting to the superior-posterior end. Second, we also report an eccentricity gradient of projections from foveal-to-peripheral V1 subregions running in the anterior-superior to posterior-inferior direction, orthogonal to the dorsal-ventral mapping. These results confirm and add to a previous diffusion MRI study (Dougherty et al. 2005) which identified a dorsal/ventral mapping of human splenial fibers. These findings yield a more detailed view of the structural organization of the splenium than previously reported and offer new opportunities to study structural plasticity in the visual system.

Introduction

In humans and other higher mammals, the right visual cortex represents the left side of the visual field and the left visual cortex represents the right side. These two halves are interconnected via axonal projections that pass through the splenium at the posterior end of the corpus callosum (Pandya et al., 1971; Rockland and Pandya, 1986; De Lacoste, 1985; Clarke and Miklossy, 1990) allowing for coverage of the visual field across the vertical midline. In humans and macaques, callosal projections are found to straddle the V1/V2 border where the vertical meridian is represented while the rest of V1 is considered to be acallosal (Van Essen et al. 1982; Kennedy et al., 1986; Kennedy and Dehay 1988; Clarke and Miklossy, 1990; Zilles and Clarke 1997). In macaques and multiple other species, many

Corresponding Author: Melissa Saenz, saenz@caltech.edu.

of these V1/V2 border connections are found to link corresponding topographic sites along the vertical meridian across the two hemispheres (cat: Segraves and Rosenquist, 1982a; Olavarria,1996; tree shrew: Bosking et al., 2000; macaque: Abel et al. 2000). Because of the topographic fidelity of these connections, it is possible that the fibers themselves are topographically organized, and that this topography would be observable at the cross-section of the splenium. However, the topographic organization of visual-callosal fibers within the splenium has not yet been clearly identified in either human or other animal models.

Occipital-callosal connections can be imaged in the human brain in vivo and non-invasively using diffusion-weighted magnetic resonance imaging and diffusion tractography. Diffusion-weighted imaging (DWI) characterizes the diffusion properties of water molecules: because water molecules diffuse preferentially along axonal tracks, the imaging of diffusion along multiple different directions allows the tracing of certain major white-matter pathways. The corpus callosum is by far the largest white matter pathway in the human brain and a variety of previous studies have validated the use of diffusion tractography for tracking cortical projections through specific regions of the corpus callosum (Huang et al., 2005; Wahl et al., 2007; Hofer et al., 2008; Park et al., 2008). Moreover, several tractography studies have identified projections from human visual cortex through the splenium (Conturo et al., 1999; Dougherty et al., 2005; Park et al., 2008; Hofer et al., 2008; Putnam et al., 2009).

Dougherty et al. (2005) specifically assessed the topographic organization of visual-callosal fibers by tracing connectivity between the splenium and several retinotopically-defined visual areas in the cortex. Their study found that ventral visual areas (ventral V1/V2, V3, V4) sent projections through the anterior-inferior corner of the splenium while dorsal visual areas (dorsal V1/V2, V3, V3A/B, V7) projected through the posterior-superior region of the splenium. Those data also hinted at an eccentricity-based topographic mapping (fovea-to-periphery) at the splenium but this was neither clear nor consistent across subjects and the authors suggested that an eccentricity mapping was likely just beyond the resolution of their methods.

The goal of our study was to more clearly measure the topographic organization of splenial projections, including both dorsal-ventral and eccentricity-based mappings, from the V1 border region using improved diffusion MRI techniques. We used high angular resolution diffusion-weighted imaging coupled with probabilistic methods (Behrens et al., 2003) to perform tractography from the splenium to retinotopic subregions of V1 at the cortical surface. Compared to conventional streamline tractography algorithms, probabilistic algorithms can progress farther into gray matter bodies (which have low directional diffusion) and are thus better suited for tracing fibers to points on the cortical surface (Behrens et al., 2003; Kinoshita et al., 2005).

Functional retinotopic mapping was used to divide V1's vertical midline representation into topographic subregions: upper and lower visual field representations and three different eccentricity bands (central, middle, and peripheral). We then classified voxels in the splenium based on each voxel's estimated connectivity profile to the different V1 surface subregions. Similar connectivity-based classification approaches have been previously applied by others across a variety of cortical areas (Behrens et al., 2003; Johansen-Berg et al., 2004; Draganski et al., 2008; Putnam et al., 2009). Generally in these studies, each voxel is classified by which of several target regions it connects to with the highest probability (i.e. winner-take-all, although see Draganski et al.). Here, we instead classified voxels based on the weighted average of their streamline connection probabilities to multiple targets so that classification reflected the overlapping connectivity estimates. Using these methods we show consistent topographic organization of V1 fibers through the human splenium. We will

discuss the application of these findings for studying structural plasticity within the human visual system.

Methods

Subjects

Six subjects (3 males, ages 21-41) participated and gave informed consent as approved by the Caltech Institutional Review Board. All subjects had normal or corrected-to-normal visual acuity and no known neurological defects.

All MRI imaging was performed on a 3 Tesla Siemens Trio scanner with an 8-channel head coil at the Caltech Brain Imaging Center. Anatomical images were acquired using a standard T1-weighted MPRAGE sequence (magnetization-prepared rapid gradient echo, 1 mm isotropic voxels) for co-registration of functional and diffusion data. The resulting co-registrations of functional to diffusion data were visually inspected for alignment of occipital cortex, specifically of the calcarine sulcus.

Functional MRI Data Collection and Analysis

Blood oxygenation-level dependent (BOLD) functional data were acquired with standard echo-planar imaging (inplane voxel size=3 mm × 3 mm, slice thickness=4 mm, nSlices =30, TR=2 s, TE=30 ms, flip angle=90 deg, field of view= 192, flip angle=80).

We used standard phase-encoded retinotopic mapping techniques to measure topographical organization within V1 (Engel et al., 1997; Sereno et al. 1995). Visual mapping stimuli were projected onto a rear-projection screen located at the end of the scanner bore which subjects viewed via an angled mirror positioned above their heads. The mapping stimuli consisted of flickering rotating wedge and expanding ring stimuli that cyclically mapped out visual space in polar angle and eccentricity.

Functional data were analyzed using Brain Voyager QX (Brain Innovation, Maastricht, The Netherlands). Pre-processing steps included motion correction, linear trend removal and temporal high-pass filtering. To facilitate visualization of the retinotopic maps, data were projected onto inflated cortical surfaces generated from each subject's anatomical data set. V1 was identified based upon identification of its retinotopic map and the polar angle phase reversal that demarcates the V1/V2 border. V1 was then partitioned into five target subregions: ventral (upper visual field quadrant) vs. dorsal (lower visual field quadrant, Figure 1A) and three eccentricity bands (central, middle, and peripheral, Figure 1B). In all subjects, the ventral and dorsal subregions (upper vs. lower visual field representations) were located on the upper and lower banks of the calcarine sulcus, respectively. The three eccentricity bands were chosen to be roughly equal in size and due to cortical magnification corresponded approximately to the following regions of visual space: central: <4 deg of visual angle, middle: 4-10 deg and peripheral: 10-18 deg.

As noted above, based on previous anatomical tracing studies in macaques and humans, V1-callosal projections are only expected within a narrow zone alongside the V1/V2 border, i.e. the vertical midline representation (Van Essen et al., 1982; Kennedy et al., 1986; Clarke and Miklossy, 1990). The exact width of this projection zone is known to vary across species and across degrees of eccentricity (Segraves and Rosenquist, 1982b; Kennedy et al.,1986; Payne, 1991; Olavarria, 1996). Rather than making an assumption about the width and shape of the projection zone in humans, for which limited data exists, we conservatively selected V1 subregions from the V1/V2 border extending fully into the acallosal center of V1. This assumption-free approach should allow us to detect V1-callosal projections in the V1/V2 border region in the most consistent manner across subjects (see further Discussion below).

After V1 subregion selection on the inflated cortical surface, each subregion was projected back into three-dimensional subject-specific native space with a thickness of 3 mm at the gray/white matter boundary (Figures 1 C,D). This subregion selection was repeated for each subject and each hemisphere for a total of 12 hemispheres. The 3-D subregion masks were exported out of Brain Voyager QX in Nifti format for subsequent tractography analysis.

Diffusion-weighted data collection and analysis

DWI data were acquired along 72 different diffusion directions using a High Angular Resolution Diffusion Imaging (HARDI) sequence (b value=1250 s/mm2, 1.9 mm isotropic voxels, TR=7800 ms TE = 104 ms, 10 volumes acquired with no diffusion weighting during the sequence). DWI data were corrected for eddy currents and head motion, skull-stripped, and registered to a T1-weighted anatomical scan for each subjects using FMRIB's software library and diffusion toolbox v2.0 (FSL, freely available at www.fmrib.ox.ac.uk/fsl). To inspect the resulting alignment between fMRI and DWI data, functionally-defined V1 subregion masks were projected onto the DWI data and visually inspected to verify that they followed the occipital gray matter surface. Because good alignment required good co-registration of both the fMRI data (from which V1 masks were generated) and the DWI data to T1-weighted anatomical data, this inspection verified good alignment and a lack of major EPI distortions within occipital cortex across anatomical, DWI and BOLD data sets.

Probabilistic tractography was performed in subject-specific native space using FMRIB's diffusion toolbox (number of diffusion directions modeled = up to 2/voxel, number of samples = 5000/voxel, curvature threshold = 0.2, maximum number of steps = 2000 step length = 0.5mm). In all tractography runs, a midline block prevented fibers from erroneously jumping from left to right occipital cortex across the hemispheric gap.

The details of the probabilistic tractography methods have been previously described (Behrens et al., 2003, 2007). Briefly, a probability distribution of fiber orientation is inferred from the data at each voxel using Bayesian estimation. Then, tractography streamlines are generated by sampling a fiber orientation from the distribution at a given voxel and drawing a line in the sampled direction towards the next voxel. Streamlines are generated a large number of times from each designated seed voxel (here 5000 streamlines/per voxel) and the probability of a streamline connection with a target is evaluated as the proportion of the total number of streamlines from a seed voxel that reach the target area. It is important to note that the probability of a streamline connection cannot be directly interpreted as the probability of an actual anatomical connection due to several limitations in fiber tracking algorithms such as distance biases (longer distances result in lower probabilities) and the difficulty of following crossing fibers (Jones, 2008).

We identified the splenium in each subject by seeding fibers across all of V1 and identifying the location where those fibers crossed the corpus callosum on the mid-sagittal slice. We then seeded fibers from the splenium voxels and classified those voxels based on their proportional streamline connection probabilities to the target subregions of V1 (5 regions per hemisphere as described above): for each splenial voxel, the number of fiber streamlines reaching each target subregion was calculated as a proportion of the total number of fiber streamlines reaching any target subregion within the classification (i.e. all of V1). To reduce noise, only voxels with a streamline connection probability of at least p=0.01 to any target (50 out of 5000 streamlines) were considered.

Two separate classifications were performed per subject per hemisphere: (1) dorsal vs. ventral; and (2) eccentricity-based (central vs. middle vs. peripheral). Each voxel was color-labeled in a graded fashion according to its proportional streamline connectivity to each of the targets regions. For example, the dorsal-ventral classification was labeled on a green-

blue scale: ventral=green [0 1 0] and dorsal=blue [0 0 1] such that if a voxel had a connectivity value of 0.9 to the ventral region and 0.1 to the dorsal region then it was assigned a color value of 0.9*[0 1 0]+0.1*[0 0 1]. The eccentricity classification was likewise labeled using a red-to-yellow scale: central = red [1 0 0], middle = orange [1 0.5 0], and periphery = yellow [1 1 0].

Results

Left and right V1 were identified using functional retinotopic mapping in all subjects. V1 was always located along the calcarine sulcus as noted by visual inspection. Subregion selection is shown for subject S1's right hemisphere in Figure 1 and for all other subjects and hemispheres in Supplementary Figures 1 and 2.

For all subjects, fiber streamlines seeded in the splenium reached V1 bilaterally via the occipital-callosal tract (Figure 2). On average, 23.3% of fibers seeded in splenium voxels reached a V1 surface mask in either hemisphere (individual subjects values: 31.9%, 21.1%, 17.2%, 28.7%, 15.1%, 26.0%). Streamlines that did not reach a V1 surface mask either: (1) terminated along the path before reaching the V1 surface, (2) reached the occipital surface surrounding V1, (3) or, in a much smaller proportion of streamlines, diverged towards other brain regions.

As shown in the top rows of Figures 3 and 4, we find a ventral to dorsal mapping of V1 fibers within the splenium with fibers from ventral V1 projecting to the inferior-anterior corner and fibers from dorsal V1 projecting to the superior-posterior end of the splenium. This pattern was consistent in 5 out 6 subjects (the exception being S5 where the mapping was unclear in both hemispheres), and is consistent with the findings of Dougherty et al. (2005).

We also find an eccentricity gradient of center-to-periphery running in the anterior-superior to posterior-inferior direction (Figures 3 and 4, bottom rows), with fibers from central (i.e. foveal) V1 projecting to the anterior-superior part of the splenium and fibers from peripheral V1 projecting to the posterior-inferior part of the splenium. As within cortex, the eccentricity gradient was orthogonal to the dorsal-ventral gradient. This pattern was consistently observed across all subjects.

In S5, the pattern of splenial connections to dorsal vs. ventral V1 was not clearly resolvable with the tractography methods used. To further investigate, we mapped S5's splenial connections to target masks representing dorsal V2/V3 vs. ventral V2/V3 (i.e. dorsal and ventral targets that are farther apart on the cortical surface). In this case, S5's dorsal/ventral mapping was more clearly resolved and was in the expected orientation, consistent with our other subjects and with Dougherty et al. (Supplementary Figure 3). This suggests that the anomalous dorsal/ventral mappings in S5 shown in Figures 3 & 4 were due to spatial limitations in the tractography methods. Acquisition of DWI data at a higher spatial resolution may improve tractography results.

Discussion

Our study identifies the structural organization of V1-callosal projections from the V1/V2 border region along both dorsal-ventral and eccentricity directions. These results add to the previous topographic mappings of Dougherty et al. by reliably demonstrating an eccentricity-based mapping of visual fibers at the splenium and confirms their mapping of dorsal vs. ventral visual fibers.

As described in the Introduction, anatomical tracer studies in macaques and post-mortem humans find V1-callosal projections only within a narrow zone along the V1/V2 border where the vertical midline is represented and the rest of V1 is considered to be acallosal (Van Essen et al., 1982; Kennedy et al., 1986; Clarke and Miklossy, 1990). The extent of this callosal-projection zone within V1 away from the V1/V2 border varies across species and across degrees of eccentricity (Segraves and Rosenquist, 1982b; Payne, 1991; Olavarria, 1996; Kennedy et al., 1986). In the macaque, callosal projections are found within V1 up to 2.5 mm away from V1/V2 border (Kennedy et al., 1986). Here, rather than making an assumption about the exact width and shape of the projection zone in humans, we conservatively selected V1 subregions from the V1/V2 border that extended fully into the acallosal center of V1. This assumption-free approach should allow us to detect V1-callosal fibers within the V1/V2 border region in the most consistent manner across subjects. It should also be noted that, while we only selected voxels within V1, given the resolution of our fMRI and DWI methods, our mapping is likely to also include some projections from within V2 near the V1/V2 border.

Comparison to previous animal studies

Although a large number of studies have examined the organization of visual-callosal projections relative to topographic sites within the two hemispheres (Van Essen et al., 1982; Segraves and Rosenquist, 1982a; Kennedy et al., 1986; Olavarria, 1996; Bosking et al., 2000), only a few studies have focused on how these fibers are organized within the splenium. As a result, the topographic organization of visual fibers within the splenium has not yet been clearly identified in either human or other animal models.

Electrophysiological recordings made by Hubel and Wiesel in the cat splenium suggested at least crude visuo-spatial topography: the receptive fields of splenial fibers from single electrode penetrations showed a tendency to cluster in space (Hubel and Wiesel, 1967). In the macaque, audioradiographic fiber tracing demonstrated distinct bundles of dorsal extrastriate vs. ventral extrastriate projections passing through the splenium: fibers from area 18 (ventral to the calcarine) ran inferior to fibers from area 19 (dorsal to the calcarine) (Rockland and Pandya, 1986). Thus, the rough topography found in the macaque seems consistent with the ventral-dorsal topography found by Dougherty et al. and with the mapping of ventral-dorsal V1 fibers found here.

Comparison to previous human diffusion MRI studies

As described above, Dougherty et al. (2005) previously traced callosal fibers from the splenium to a broader region of visual cortex in four human subjects and reported that ventral visual areas (ventral V1/V2, V3, V4) send projections through the anterior-inferior corner of the splenium, while dorsal visual areas (dorsal V1/V2, V3, V3A/B, V7) send projections through a larger superior-posterior band. Here we mapped splenial projections from within V1, and identified a ventral-dorsal mapping. The direction of this mapping was consistent with Dougherty et al.'s ventral-dorsal mapping and consistent with V1's continuous topographic location between the ventral and dorsal extrastriate areas on the cortical surface.

In addition to the dorsal-ventral mapping, we also report a splenial eccentricity mapping of fovea-to-periphery from the anterior-superior corner to the posterior-inferior end of the splenium. Dougherty et al.'s data hinted at a similar eccentricity mapping but it was not clearly resolvable and this mapping was most likely just above the limits of the resolution of their methods. Our clearer demonstration of visual topographic mappings through the splenium may be attributed to the higher angular resolution of our imaging as well as our use of probabilistic tractography methods. Compared to deterministic streamline

tractography algorithms, probabilistic algorithms can progress farther into gray matter bodies (which have low directional diffusion) and are thus better suited for tracing fibers to points on the gray matter cortical surface (Behrens et al., 2003; Kinoshita et al., 2005).

Future Applications

It is important to recognize that diffusion tractography has many limitations compared with invasive tracer injection techniques. Diffusion tractography cannot identify the direction of connections, has difficulty following projections through regions of fiber crossing, and can mistakenly follow intervening paths (Jones, 2008). Thus, current methods are most reliable for tracing dominant axonal tracts like the visual-callosal pathway whose existence is already well established. Diffusion tractography methods are in an active state of development and the probabilistic algorithm employed here (Behrens et al., 2003; Behrens et al., 2007) represents one approach out of several in the field that are yielding improved fiber tracing results (Parker et al., 2003; Hagmann et al., 2007; Sherbondy et al., 2008). Much room for innovation remains and will continue to be pursued while diffusion tractography remains the only option for studying white matter pathways non-invasively in the human brain.

The topographic mapping of V1-callosal projections offers new opportunities to study plasticity of white matter pathways by providing a reliable framework for studying potentially abnormal connectivity patterns in certain patient groups. For example, people with early visual loss show dramatic functional reorganization of the visual cortex (Sadato et al., 1996; Saenz et al., 2008; Merabet and Pascual-Leone, 2010) and it is unknown whether visual-callosal reorganization may also occur. Although most white matter connections develop early in life there is increasing evidence that white matter connectivity can be altered by experience (Fields, 2008; Scholz et al., 2009) and many effects of aging on white matter integrity have been established (Westlye et al. 2009, Peters et al., 2009). Despite wide variation in the size of V1 across individuals (Dougherty et al. 2003), V1 location can be well estimated within individual subjects by its anatomical location along the calcarine sulcus and surrounding cortical folding patterns (Hinds et al., 2009; Hinds et al., 2008). Thus, the analysis presented here could equivalently be carried out using anatomical estimates of V1 when functional mapping is not possible.

Supplementary Material

Refer to Web version on PubMed Central for supplementary material.

Acknowledgments

This work was supported by the NEI (61-4892), Dana Innovations in Neuroimaging and The Mathers Foundation. We thank Christof Koch for comments on the manuscript.

References

Abel PL, O'Brian BJ, Olavarria JF. Organization of callosal linkages in visual area V2 of macaque monkey. Journal of Comparative Neurology. 2000; 428:278–93. [PubMed: 11064367]

Behrens TEJ, Johansen-Berg H, et al. Non-invasive mapping of connections between human thalamus and cortex using diffusion imaging. Nature Neuroscience. 2003; 6:750–757.

Behrens TEJ, Woolrich MW, Jenkinson M, Johansen-Berg H, Nunes RG, Clare S, Matthews PM, Brady JM, Smith SM. Characterization and propagation of uncertainty in diffusion-weighted MR imaging. Magnetic Resonance in Medicine. 2003; 50(5):1077–1088. [PubMed: 14587019]

Behrens TEJ, Johansen Berg H, Jbabdi S, Rushworth MFS, Woolrich MW. Probabilistic diffusion tractography with multiple fibre orientations: What can we gain? NeuroImage. 2007; 34:144–155. [PubMed: 17070705]

Bosking WH, Kretz R, Pucak ML, Fitzpatrick D. Functional specificity of callosal connections in tree shrew striate cortex. The Journal of Neuroscience. 2000; 20:2346–59. [PubMed: 10704509]

Clarke S, Miklossy J. Occipital cortex in man: Organization of callosal connections, related myelo- and cytoarchitecture, and putative boundaries of functional visual areas. The Journal of Comparative Neurology. 1990; 298:188–214. [PubMed: 2212102]

Conturo TE, Lori NF, Cull TS, Akbudak E, Snyder AZ, Shimony JS, McKinstry RC, Burton H, Raichle ME. Tracking neuronal fiber pathways in the living human brain. Proceedings of the National Academy of Sciences. 1999; 96:10422–10427.

Dougherty RF, Koch VM, Brewer AA, Fischer B, Modersitzki J, Wandell BA. Visual field representations and locations of visual areas V1/2/3 in human visual cortex. Journal of Vision. 2003; 3(1):586–98. [PubMed: 14640882]

Dougherty RF, Ben-Shachar M, Bammer R, Brewer AA, Wandell BA. Functional organization of human occipital-callosal fiber tracts. Proceedings of the National Academy of Sciences. 2005; 102:7350–7355.

Draganski B, Kherif F, Kloppel S, Cook PA, Alexander DC, Parker GJM, Deichmann R, Ashburner J, Frackowiak RSJ. Evidence for Segregated and Integrative Connectivity Patterns in the Human Basal Ganglia. The Journal of Neuroscience. 2008; 28:7143–7152. [PubMed: 18614684]

Engel SA, Glover GH, Wandell BA. Retinotopic organization in human visual cortex and the spatial precision of functional MRI. Cerebral Cortex. 1997; 7(2):181–192. [PubMed: 9087826]

Fields RD. White matter in learning, cognition, and psychiatric disorders. 2008; 31:61–370.

Hagmann P, Kurant M, Gigandet X, Thiran P, Wedeen Van J, Meuli R, Thiran JP. Mapping human whole-brain structural networks with diffusion MRI. PloS One. 2007; 2(7):e597. [PubMed: 17611629]

Hinds O, Polimeni JR, Rajendran N, Balasubramanian M, Amunts K, Zilles K, Schwartz EL, Fischl B, Triantafyllou C. Locating the functional and anatomical boundaries of human primary visual cortex. NeuroImage. 2009; 46:915–922. [PubMed: 19328238]

Hinds OP, Rajendran N, Polimeni JR, Augustinack JC, Wiggins G, Wald LL, Rosas HD, Potthast A, Schwartz EL, Fischl B. Accurate prediction of V1 location from cortical folds in a surface coordinate system. NeuroImage. 2008; 39(4):1585–1599. [PubMed: 18055222]

Hofer S, Merboldt KD, Tammer R, Frahm J. Rhesus Monkey and Human Share a Similar Topography of the Corpus Callosum as Revealed by Diffusion Tensor MRI In Vivo. Cerebral Cortex. 2008; 18:1079–1084. [PubMed: 17709556]

Huang H, Zhang J, Jiang H, Wakana S, Poetscher L, Miller MI, van Zijl Peter CM, Hillis AE, Wytik R, Mori S. DTI tractography based parcellation of white matter: Application to the mid-sagittal morphology of corpus callosum. NeuroImage. 2005; 26:195–205. [PubMed: 15862219]

Hubel DH, Wiesel TN. Cortical and callosal connections concerned with the vertical meridian of visual fields in the cat. Journal of Neurophysiology. 1967; 30:1561–1573. [PubMed: 6066454]

Johansen-Berg H, Behrens TEJ, Robson MD, Drobnjak I, Rushworth MFS, Brady JM, Smith SM, Higham DJ, Matthews PM. Changes in connectivity profiles define functionally distinct regions in human medial frontal cortex. Proceedings of the National Academy of Sciences. 2004; 101:13335–13340.

Jones DK. Studying connections in the living human brain with diffusion MRI. Cortex. 2008; 44:936–52. [PubMed: 18635164]

Kennedy H, Dehay C, Bullier J. Organization of the callosal connections of visual areas V1 and V2 in the macaque monkey. The Journal of Comparative Neurology. 1986; 247:398–415. [PubMed: 3088065]

Kennedy H, Dehay C. Functional implication of the anatomical organization of the callosal projections of visual areas V1 and V2 in the macaque monkey. Behavioural Brain Research. 1988; 29:225–36. [PubMed: 3166700]

Kinoshita M, Yamada K, Hashimoto N, Kato A, Izumoto S, Baba T, Maruno M, Nishimura T, Yoshimine T. Fiber-tracking does not accurately estimate size of fiber bundle in pathological

condition: initial neurosurgical experience using neuronavigation and subcortical white matter stimulation. NeuroImage. 2005; 25:424–429. [PubMed: 15784421]

de Lacoste MC, Kirkpatrick JB, Ross ED. Topography of the human corpus callosum. Journal of Neuropathology and Experimental Neurology. 1985; 44:578–591. [PubMed: 4056827]

Merabet LB, Pascual-Leone A. Neural reorganization following sensory loss: the opportunity of change. Nature Reviews Neuroscience. 2010; 11:44–52.

Olavarria JF. Non-mirror-symmetric patterns of callosal linkages in areas 17 and 18 in cat visual cortex. The Journal of Comparative Neurology. 1996; 366:643–655. [PubMed: 8833114]

Pandya DN, Karol EA, Heilbronn D. The topographical distribution of interhemispheric projections in the corpus callosum of the rhesus monkey. Brain Research. 1971; 32:31–43. [PubMed: 5000193]

Park HJ, Kim JJ, Lee SK, Seok JH, Chun J, Kim DI, Lee JD. Corpus callosal connection mapping using cortical gray matter parcellation and DT-MRI. Human Brain Mapping. 2008; 29:503–516. [PubMed: 17133394]

Parker G, Hamied JM, Haroon A, Wheeler-Kingshott CAM. A framework for a streamline-based probabilistic index of connectivity (PICo) using a structural interpretation of MRI diffusion measurements. Journal of Magnetic Resonance Imaging. 2003:242–254. [PubMed: 12884338]

Payne BR. Visual-field map in the transcallosal sending zone of area 17 in the cat. Visual Neuroscience. 1991; 7:201–219. [PubMed: 1721530]

Peters A. The effects of normal aging on myelinated nerve fibers in monkey central nervous system. Fronteirs in Neuroanatomy. 2009; 3(11)

Putnam MC, Steven MS, Doron KW, Riggall AC, Gazzaniga MS. Cortical Projection Topography of the Human Splenium: Hemispheric Asymmetry and Individual Differences. Journal of Cognitive Neuroscience. 2009; 0:1–8.

Rockland KS, Pandya DN. Topography of occipital lobe commissural connections in the rhesus monkey. Brain Research. 1986; 365:174–178. [PubMed: 3947983]

Sadato N, Pascual-Leone A, Grafman J, Ibañez V, Deiber MP, Dold G, Hallett M. Activation of the primary visual cortex by Braille reading in blind subjects. Nature. 1996; 380:526–528. [PubMed: 8606771]

Saenz M, Lewis LB, Huth AG, Fine I, Koch C. Visual Motion Area MT+/V5 Responds to Auditory Motion in Human Sight-Recovery Subjects. The Journal of Neuroscience. 2008; 28:5141–5148. [PubMed: 18480270]

Scholz J, Klein MC, Behrens TEJ, Johansen-Berg H. Training induces changes in white-matter architecture. Nature Neuroscience. 2009; 12:1370–1371.

Segraves MA, Rosenquist AC. The afferent and efferent callosal connections of retinotopically defined areas in cat cortex. The Journal of Neuroscience. 1982a; 2:1090–1107. [PubMed: 6180150]

Segraves MA, Rosenquist AC. The distribution of the cells of origin of callosal projections in cat visual cortex. The Journal of Neuroscience. 1982b; 2:1079–1089. [PubMed: 6180149]

Sereno MI, Dale AM, Reppas JB, Kwong KK, Belliveau JW, Brady TJ, Rosen BR, Totell RB. Borders of multiple visual areas in humans revealed by functional magnetic resonance imaging. Science. 1995; 5212:889–893. [PubMed: 7754376]

Sherbondy AJ, Dougherty RF, Ben-Shachar M, Napel S, Wandell BA. ConTrack: Finding the most likely pathways between brain regions using diffusion tractography. Journal of Vision. 2008; 8:1–16.

Van Essen DC, Newsome WT, Bixby JL. The pattern of interhemispheric connections and its relationship to extrastriate visual areas in the macaque monkey. The Journal of Neuroscience. 1982; 2:265–283. [PubMed: 7062108]

Wahl M, Lauterbach-Soon B, Hattingen E, Jung P, Singer O, Volz S, Klein JC, Steinmetz H, Ziemann U. Human Motor Corpus Callosum: Topography, Somatotopy, and Link between Microstructure and Function. The Journal of Neuroscience. 2007; 27:12132–12138. [PubMed: 17989279]

Westlye LT, Walhovd KB, Dale AM, Bjørnerud A, Due-Tønnessen P, Engvig A, Grydeland H, Tamnes CK, Ostby Y, Fjell AM. Life-Span Changes of the Human Brain White Matter: Diffusion Tensor Imaging (DTI) and Volumetry. Cerebral Cortex. 2009

Zilles, K.; Clarke, S. Architecture, connectivity and transmitter receptors of human extrastriate cortex. Comparison with non-human primates. In: Rockland, KS.; Kaas, JH.; Peters, A., editors. Cerebral Cortex: Extrastriate Cortex in Primates. Plenum Press; New York: 1997. p. 673-742.

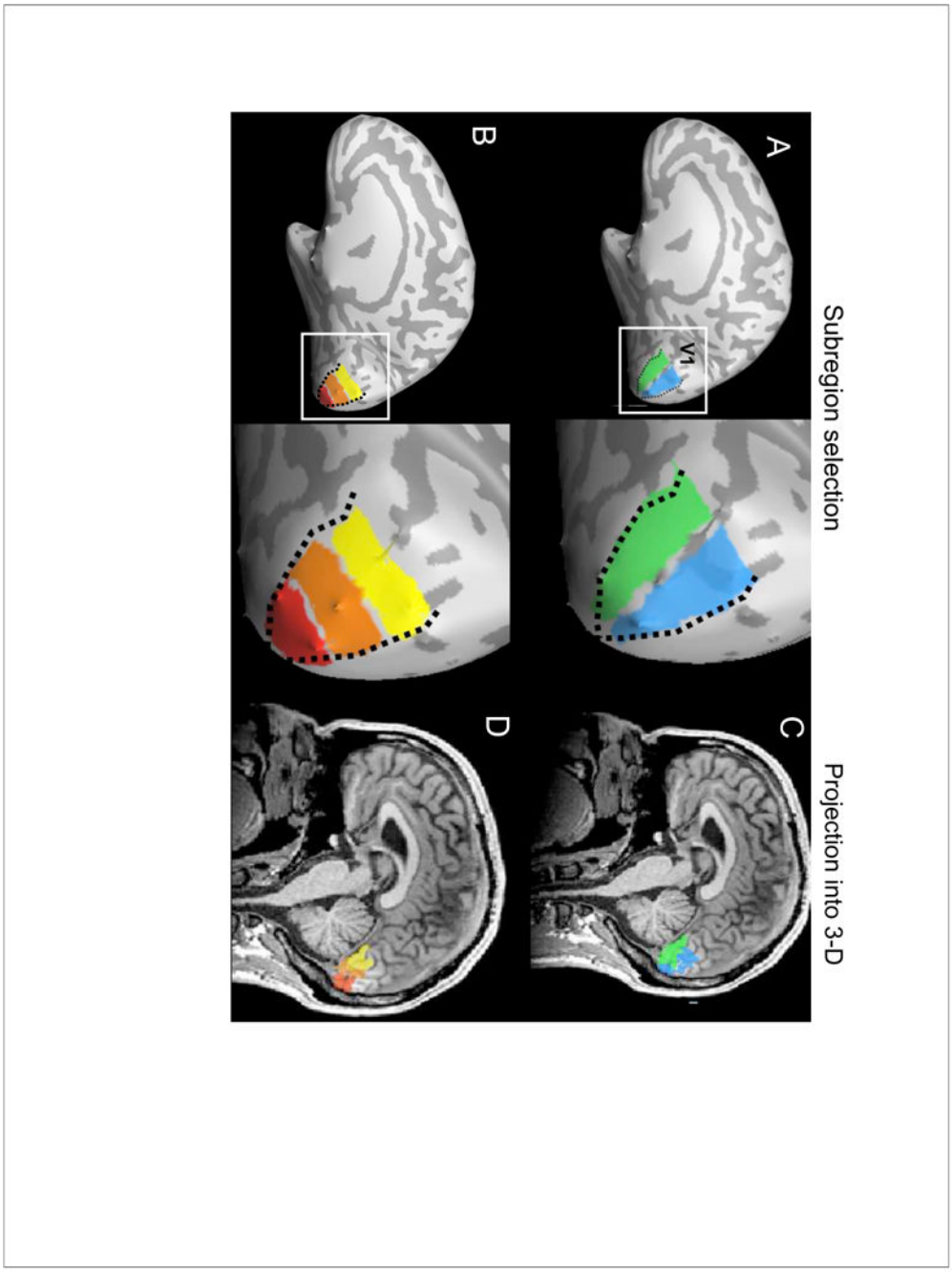

Figure 1. Topographic subregion selection in V1

(A) Inflated right-hemisphere surface of one example subject to show subregion selection in V1. A dotted line shows the V1/V2 border, as estimated by standard functional MRI retinotopic mapping. In macaques and humans, V1-callosal projections are found only within a narrow zone along the V1/V2 border where the vertical midline is represented and the rest of V1 is considered to be acallosal. In our study rather than making an assumption about the exact width and shape of this projection zone, we conservatively selected subregions from the V1/V2 border extending fully into the acallosal center of V1. This assumption-free approach should allow us to detect all V1-callosal fibers in the most consistent manner across subjects. Based on the functional mapping, we divided V1 into

upper (green) and lower (blue) visual field representations and into (B) three different eccentricity bands representing central, middle, and peripheral visual fields. C,D) After selection on the inflated surface, subregions were projected back into each subject's three-dimensional native space at the gray/white matter boundary. These V1 subregion masks were used as targets in the subsequent tractography analysis.

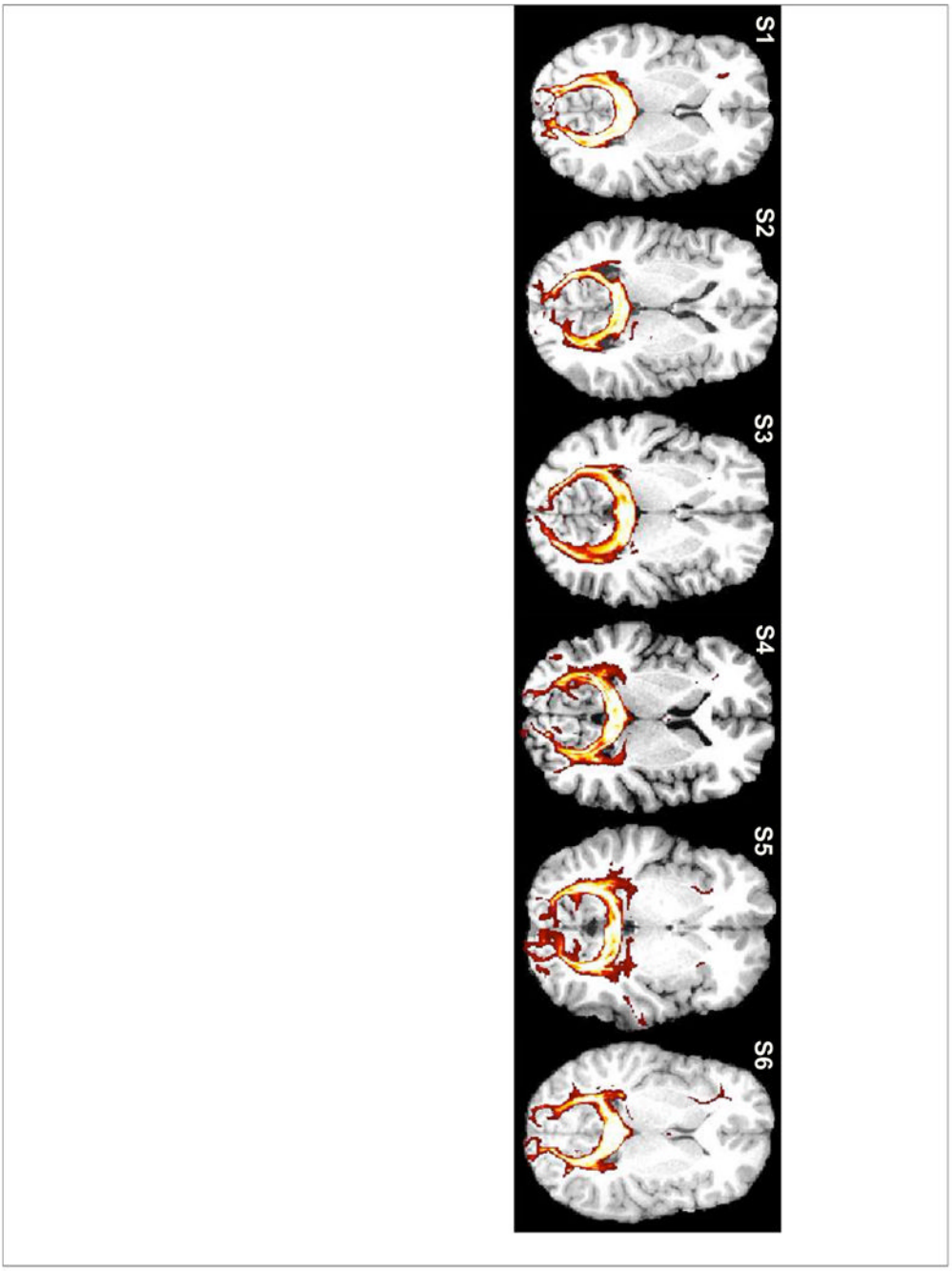

Figure 2. Occipital-callosal fiber tracts

Tractography streamlines seeded in the splenium reached occipital cortex bilaterally. Voxels are color-coded by the number of streamlines passing through the voxel from from 50 (red) to 5000 (whilte).

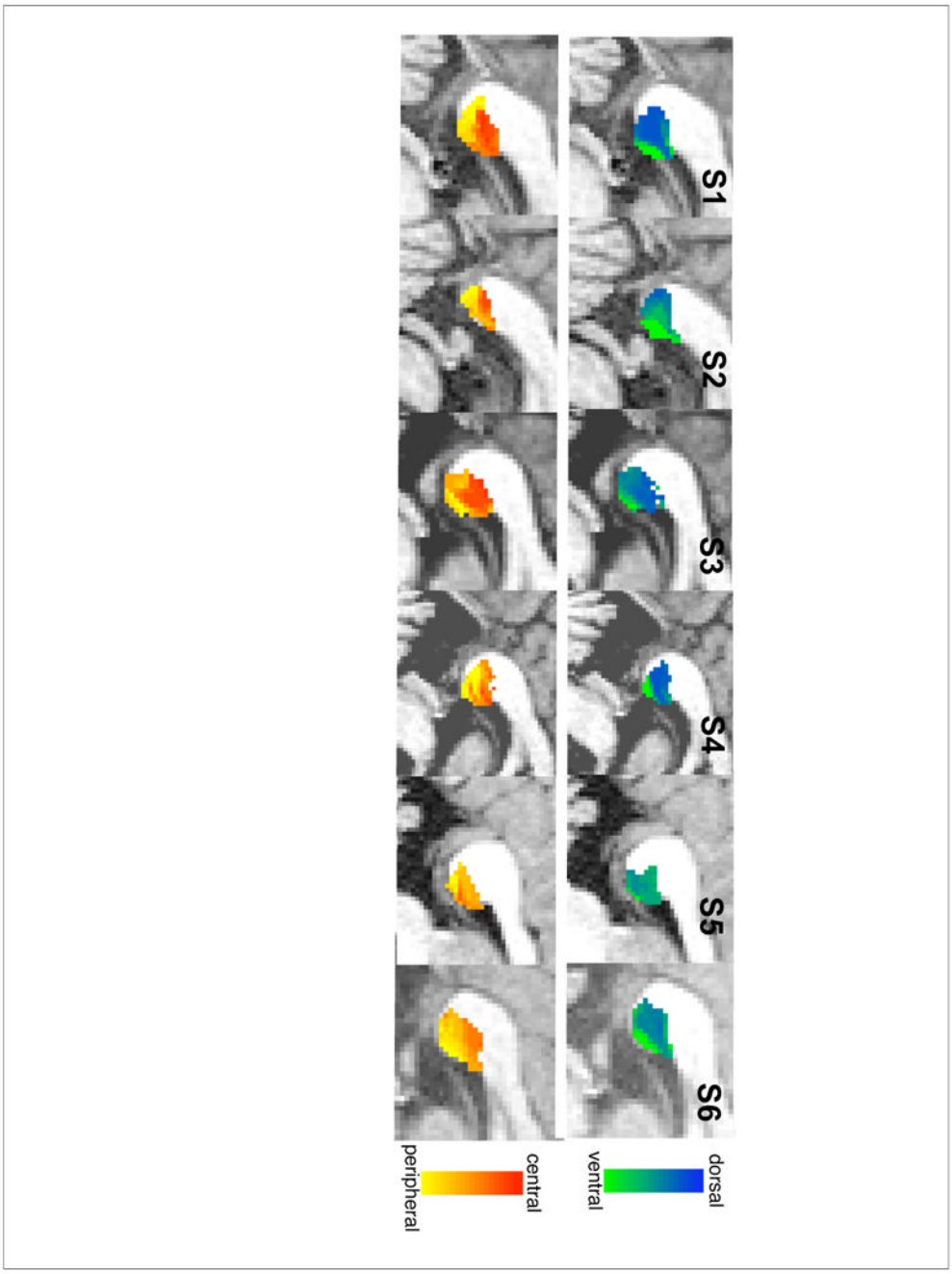

Figure 3. Projections from Splenium to left hemisphere V1

Each splenium voxel is classified based upon the proportional number of its streamline connections reaching V1 ventral (green) vs. V1 dorsal (blue) subregions in the top row, and V1 central (red) vs. middle (orange) vs. peripheral (yellow) subregions in the bottom row.

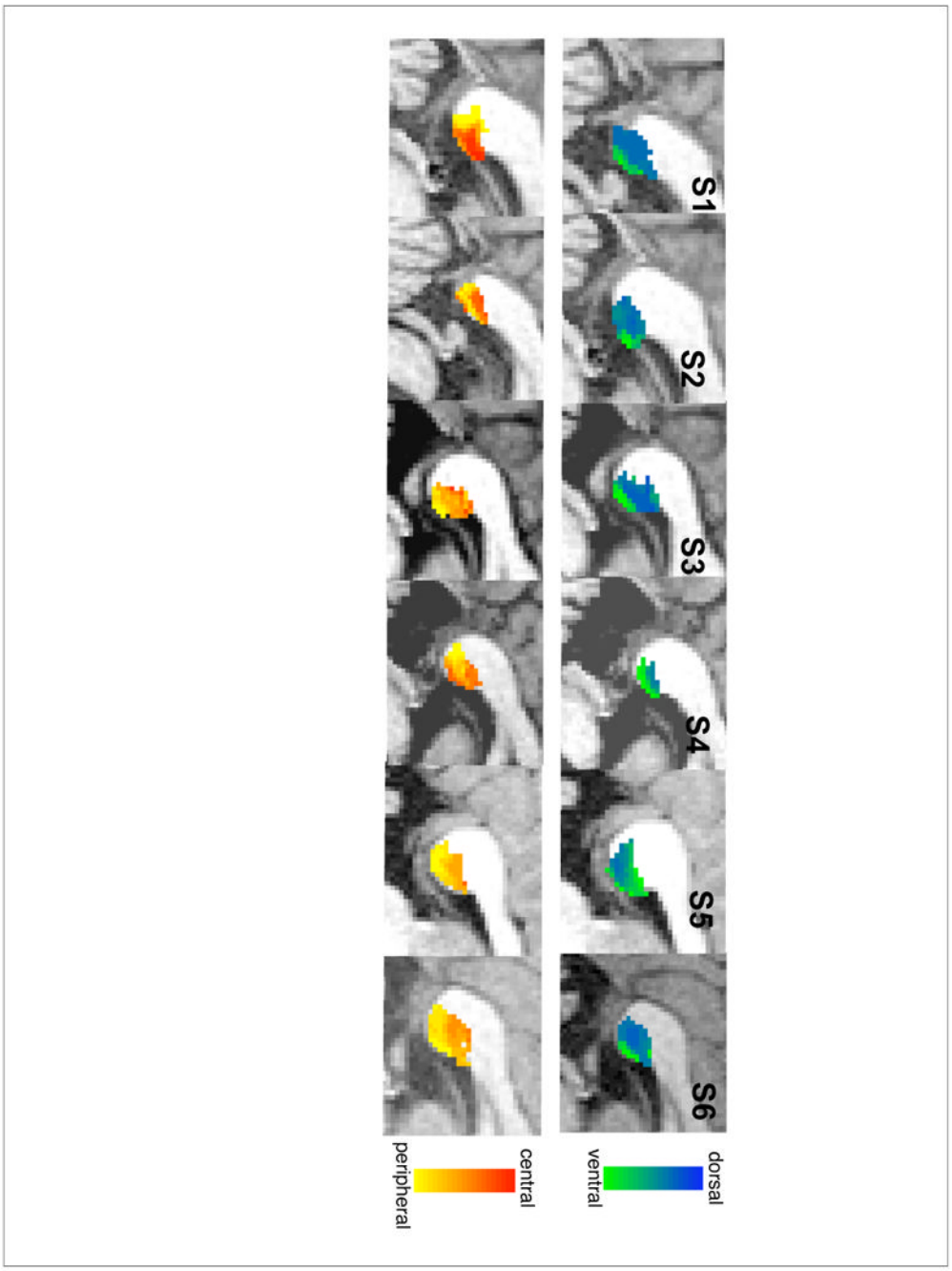

Figure 4. Projections from Splenium to right hemisphere V1

Each splenium voxel is classified based upon the proportional number of its streamline connections reaching V1 ventral (green) vs. V1 dorsal (blue) subregions in the top row, and V1 central (red) vs. middle (orange) vs. peripheral (yellow) subregions in the bottom row.